Electrical Power and Energy Systems 97 (2018) 17–27

Contents lists available at ScienceDirect

Electrical Power and Energy Systems

journal homepage: www.elsevier.com/locate/ijepes

Analytical assessment of voltage support via reactive power from new electric vehicles supply equipment in radial distribution grids with voltage-dependent loads

Antonio Zecchino, Mattia Marinelli*

Center for Electric Power and Energy, Technical University of Denmark, DTU Risø Campus, Frederiksborgvej 399, 4000 Roskilde, Denmark

ARTICLE INFO

Keywords:
Distribution grid
Electric vehicle
Electric vehicle supply equipment
Reactive power
Voltage support

ABSTRACT

Grid operators have to cope with secure electric vehicles integration in the power system, which may lead to violations of the allowed voltage band. This work intends to provide an analytical assessment and guidelines for distribution system operators when evaluating new electric vehicle supply equipment installations with fast charging capability in existing low voltage distribution feeders. The aim is to prevent the voltage to exceed the permitted values when charging at high power, by exploiting the effect of reactive power. The contribution of each power component in distribution grids is analyzed, including the loads' voltage-dependency, which influences the effectiveness of reactive power control. The proposed guidelines indicate the amount of capacitive reactive power that an individual electric vehicle supply equipment is expected to provide, in order to effectively manage the voltage rise. The proposed method is validated on the Cigrè benchmark low voltage distribution network as well as on a real Danish low voltage grid.

1. Introduction

The increasing success of electric vehicles (EVs) is bringing new challenges to power system operators. On the one hand, great research effort is made on smart integration solutions of large amount of EVs in the power system, such as aggregation strategies for smart EV charging aim at making EVs a reliable source of system-wide ancillary services [1–3]. On the other hand, to evaluate the practical feasibility of such solutions, the technical capabilities of series-produced EVs in performing smart charging are of high interest too [4,5]. However, since mostly connected at a low voltage (LV) level, one of the most challenging aspects of the integration of EVs in the power system is the impact on distribution grids [6,7].

Distribution system operators (DSOs) should be always able to operate their distribution networks assuring standard-compliant levels of power quality, according to the European technical standard EN 50160 [8]. When connected to electric vehicles supply equipment (EVSE), EVs behave as large concentrated loads. Thus, they may cause technical issues on the electrical infrastructure, such as overloading conditions both in distribution transformers and feeders and drastic power quality worsening. Unless opting for grid reinforcement solutions, a massive penetration of EVs in distribution networks may force DSOs to rely on smart EV charging.

In general, reactive power provision can – to a certain extent – mitigate local voltage issues in distribution networks [9]. In case of small distributed generation plants connected at low voltage levels such as photovoltaics (PVs), grid technical standards require reactive power capability to the inverter-interfaced units [10–12]. Many studies have proved the effectiveness of such capabilities in voltage support in active distribution networks [13,14]. Similarly, it is expected that there might by a need for DSOs to require voltage support capability also to the new EVSEs.

Under a technical feasibility point of view, many studies propose new on-board chargers design and investigate the barriers within the power electronics in applying reactive power solutions [15–17]. Among others, [17] presents an analysis of the technical performance of a conventional unidirectional on-board charger during bidirectional four-quadrant operation, showing how reactive power exchange could be achieved without any considerable changes in the converter type and size. Furthermore, many other studies deal with the development of off-board chargers capable of reactive power operation, showing possible designs and layouts of such technologies [18,19]. Hence, given the mentioned concrete technical feasibility, it is of paramount interest to perform assessment studies upon the effective contribution of such reactive power voltage regulation strategies by charging EVs.

Among other possible control techniques, many reactive power

* Corresponding author.
E-mail address: matm@elektro.dtu.dk (M. Marinelli).

http://dx.doi.org/10.1016/j.ijepes.2017.10.034
Received 10 April 2017; Received in revised form 14 September 2017; Accepted 25 October 2017
Available online 04 January 2018
0142-0615/

Nomenclature

List of symbols

$\overline{E_1}$	phase-neutral voltage phasor at the starting terminal of the line
$\overline{E_2}$	phase-neutral voltage phasor at the ending terminal of the line
E_1	phase-neutral voltage magnitude at the starting terminal of the line
E_2	phase-neutral voltage magnitude at the ending terminal of the line
$\overline{\Delta E}$	complex voltage drop along the generic distribution line
R_l	resistance of the generic distribution line
X_l	reactance of the generic distribution line
P	total active power absorbed by the customer
Q	total reactive power absorbed by the customer
$\overline{I}$	phasor current flowing along the line
I_r	real component of the current flowing along the line
I_i	imaginary component of the current flowing along the line
a_0, a_1, a_2, b_0, b_1, b_2	load voltage dependence modelling coefficients
P_{EV}	electric vehicle active power
Q_{EV}	electric vehicle reactive power
P_{load}	load active power
Q_{load}	load reactive power
$P_{load.0}$	load active power at nominal voltage condition
$Q_{load.0}$	load reactive power at nominal voltage condition
$\cos\varphi_{EV}$	power factor of the charging electric vehicle
$\cos\varphi_{load}$	power factor of the load
$S_{sc.grid}$	external grid short-circuit power
	external grid resistance referred to the low voltage level
X_{grid}	external grid reactance referred to the low voltage level
R/X_{grid}	resistance over reactance ratio of the transformer
$S_{n.trafo}$	transformer nominal power
$S_{sc.trafo}$	transformer short-circuit power
$Z_{sc.trafo}$	transformer short-circuit impedance
$v_{sc\%.trafo}$	transformer short-circuit voltage
R_{trafo}	transformer resistance referred to the low voltage level
X_{trafo}	transformer reactance referred to the low voltage level
R/X_{trafo}	resistance over reactance ratio of the transformer
$R_{LVfeeder}$	low voltage feeder resistance
$X_{LVfeeder}$	low voltage feeder reactance
$RX_{LVfeeder}$	resistance over reactance ratio of the low voltage feeder

control strategies based on solution of optimization problems are proposed in the literature, both with centralized and decentralized control structure. In general, centralized control approaches for this kind of voltage regulation at LV distribution level [20,21] may result in huge amount of data that need to be transported from smart meters to a centralized control room for the elaboration of the proper control signal to be dispatched back to the units. Therefore, in many volt-VAR optimization works it is preferred to rely on decentralized logics, avoiding the need for complex data management [22–25].

Independently on the control logic applied, many other studies have been conducted with the aim to demonstrate the potentials of distributed EV chargers control to solve local voltage issues and allowing high EV penetration to be technically acceptable, deferring the need for grid reinforcement [26–30]. In [26] and [27] the positive effects of reactive power support by EVs applying voltage-dependent reactive power strategies is analyzed. An implementation of a bi-directional EVSE controller is developed in [28], which proposes a control logic able to regulate the bus voltage by exchanging reactive power, while maintaining a given DC-link voltage for the designed charging station. In [29] an example of the impact in the power grid is evaluated by implementing different reactive power control logics such as fixed power factor, power factor as function of either active power or local voltage, and an hysteresis control. An innovative reactive power capability curve as function of both active power and local voltage is proposed in [30], where EVs are considered to be single-phase connected, thus unbalance conditions are evaluated.

The above-listed works do present the positive effects on local voltage by reactive power provision from EVs; however, all these study cases are validated in single distribution grids. As the effectiveness of such controllers depends on the electrical characteristics of the power system, it is of high interest to evaluate their influence in different grid cases. In this respect, in [31] the effectiveness of reactive power control from PV inverters is evaluated with respect to different R/X grid characteristic, and it is shown how, depending on the grid characteristics, over-voltages can be reduced.

Similarly, it is expected that for installations of new commercial EVSEs with fast charging capability in existing LV distribution feeders, the reactive power needed to prevent undesired under-voltages depends on the grid characteristic. Within this context, in [32] we have investigated the influence of the single distribution grid components on the reactive power effect. Specifically, the proposed analysis demonstrates that both the MV/LV transformer and the MV grid (unless extremely weak) have marginal influence on the effects of reactive power on the voltage. Moreover, it is also found that the R/X ratio of the LV feeder does not significantly influence the results, whereas an important role is played by the absolute values of R and X, i.e., the LV feeder length. In this work we aim at extending and enhancing the investigation proposed in [32], by including the voltage-dependency of the loads in the analytical formulation, as well as carrying out a validation on different grids. The reactive power effects on the local voltage are evaluated in case of different load models in terms of inductive power factor as well as voltage-dependent behaviour.

So, the identified research questions we are trying to answer with these contributions are: *how much is it possible to exploit the potential flexibility of EV fast chargers in providing reactive power for voltage control in LV distribution grids? Which guidelines can be given to DSOs in terms of the amount of reactive power that an individual EV must be able to provide?*

The novelty lies on the provision of such guidelines for DSOs, applicable to different types of customers, e.g., residential, commercial, and industrial. The proposed method is to be seen as an assessment criterion when DSOs have to evaluate requests for installation of new EV fast chargers in LV networks. The proposed analytical formulation has been validated by implementing equations in MATLAB. The further validation has been carried out by running load flow calculations in the power system simulation tool DIgSILENT PowerFactory on the LV Cigrè residential radial benchmark [33], as well as on a real Danish LV distribution network previously utilized for other EV integration-related studies [30].

The paper is structured as follows. Section 2 presents the analytical formulation for assessing reactive power effects in distribution grids. Section 3 outlines the methodology to evaluate the contribution of the single power system components. In Section 4 a detailed sensitivity analysis including the load models is presented. Section 5 reports the validation of the proposed methodology. Conclusions are reported in Section 6.

2. Voltage drop assessment in distribution grids

Although reactive power management for voltage support has major effects at HV/MV levels due to low R/X ratios (0.1–0.2), in LV distribution networks (average R/X ratio of 0.5–5) it is anyway seen as a feasible mean to maintain voltages within the allowed limits of ± 10%

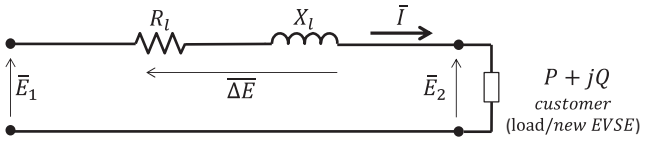

Fig. 1. Single-phase equivalent circuit of a three-phase LV line.

of the nominal value [8]. In fact, the operation of modern distribution grids is challenged by the increasing penetration of renewable energy resources as well as new electrical loads, such as EVs [26,30]. For instance, in most of the European countries for residential PV installations connected to LV distribution grids, voltage regulation by reactive power provision is already required [10–12]. Similarly, the EV charging process could be performed by utilizing a capacitive power factor, i.e., injecting reactive power, to avoid under-voltages.

In distribution grids the transversal parameters conductance and susceptance are negligible for LV levels. All the grids with negligible transversal parameters can be represented by an R-L circuit as the one in Fig. 1, which shows the single-phase equivalent circuit of a balanced three-phase line, where R_l and X_l are the longitudinal parameters of the distribution line, $\overline{E_1}$ and $\overline{E_2}$ the phase-neutral voltages at the two terminals, and $\overline{\Delta E}$ the voltage drop along the line. The assumption of a balanced three-phase system is motivated by the fact that the new fast-charger has a three-phase connection, thus not introducing any additional unbalance components, such as the one utilized in the field trial mentioned in [34].

The apparent power absorbed by the customer at the end of the line $\bar{S}$, can be expressed as in Eq. (1), where $\bar{I}^*$ is the conjugate of the drawn complex current.

$$\bar{S} = 3\overline{E_2} * \bar{I}^* = P + jQ \tag{1}$$

From (1) it is possible to obtain $\bar{I}$ as function of the voltage $\overline{E_2}$ (taken as reference), and of the real and imaginary components of $\bar{S}$, i.e., P and Q, respectively. This formulation is reported in Eq. (2).

$$\bar{I} = \left(\frac{\bar{S}}{3\overline{E_2}}\right)^* = \frac{\bar{S}^*}{3\overline{E_2}^*} = \frac{(P + jQ)^*}{3E_2} = \frac{P - jQ}{3E_2} \tag{2}$$

Eq. (3) reports the complex phasor $\bar{I}$, whose real and imaginary components I_r and I_i are made explicit in Eqs. (4) and (5).

$$\bar{I} = I_r + jI_i \tag{3}$$

$$I_r = \frac{P}{3E_2} \tag{4}$$

$$I_i = \frac{-Q}{3E_2} \tag{5}$$

Note that the sign of the real component of the current I_r indicates whether the customer is absorbing or injecting power. In case of an EV, this means it is charging or discharging, corresponding to the I/IV or II/III quadrants of the P-Q 4-quadrant EVSE converter operating scheme of Fig. 2. The phase angle φ and therefore the imaginary component I_i, shows if the customer is exchanging inductive (positive) or capacitive (negative) reactive power, which corresponds to the I/II or the III/IV quadrant, respectively. As it can be seen in the phasor diagram in Fig. 3, $\overline{E_2}$ is considered as reference, and therefore $\overline{E_1}$ and $\bar{I}$ are shifted by ε and φ, respectively.

The complex voltage at the starting terminal of the line $\overline{E_1}$ is equal to $\overline{E_2}$ with the addition of the complex voltage drop along the line $\overline{\Delta E}$, as in Eq. (6). $\overline{\Delta E}$ is the complex product of current $\bar{I}$, which can be written as in (2), and the line impedance $\overline{Z_l}$, which can be written as $(R_l + jX_l)$.

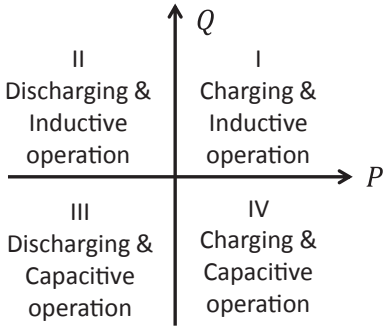

Fig. 2. 4-quadrant EVSE converter operating scheme (load convention).

$$\overline{E_1} = \overline{E_2} + \overline{\Delta E} = \overline{E_2} + \bar{I} * \overline{Z_l} = E_2 + \frac{P - jQ}{3E_2} * (R_l + jX_l)$$
$$= \left(E_2 + \frac{PR_l + QX_l}{3E_2}\right) + j\left(\frac{PX_l - QR_l}{3E_2}\right) \tag{6}$$

From Eq. (6), the voltage magnitude E_1 and angle ε at the starting bus can be derived as in Eqs. (7) and (8), respectively [35].

$$|\overline{E_1}| = E_1 = [(Re(\overline{E_1}))^2 + (Im(\overline{E_1}))^2]^{0.5}$$
$$= \left[E_2^2 + \frac{2}{3}(PR_l + QX_l) + \frac{(P^2 + Q^2)(R_l^2 + X_l^2)}{9E_2^2}\right]^{0.5} \tag{7}$$

$$\varepsilon = \tan^{-1}\left[\frac{Im(\overline{E_1})}{Re(\overline{E_1})}\right] \tag{8}$$

In the proposed analytical assessment the module of E_1 (i.e., the length *OB* of Fig. 3) is set to a particular value independently of its angle ε, which is thus not included in the final formulation. In fact, the proposed formulation enables us to estimate the actual magnitude of the voltage E_2 independently from its shift over E_1. In comparison to the traditional way of simplifying the formulation by neglecting the imaginary part of (6) (thus considering only the projection of E_1 on the real axis, i.e., *OH*), this formulation takes into account the entire magnitude of the vector E_1, i.e., *OB* = *OC*. Although it still differs from the traditional exact complex estimation of the line voltage drop, crucial when assessing grid losses, still it represents a precise way for estimating the impact on the local voltage of new EVSEs installations.

By combining Eqs. (2) and (7), and with reference to the phasor diagram in Fig. 3, it is possible to express the magnitude of E_2 as in Eq. (9), i.e., as function of E_1, the real and imaginary components of the current (I_r and I_i), and the line impedance ($R_l + jX_l$):

$$E_2 = [E_1^2 - (I_i R_l + I_r X_l)^2]^{0.5} - I_r R_l + I_i X_l \tag{9}$$

In case of capacitive reactive power (negative Q, which means positive I_i) the voltage drop due to active current absorption $-I_r R_l$ is partially compensated by the voltage rise due to the reactive current $+ I_i X_l$. Thus, in order to support the grid during EV charging, instead of reducing the active charging power and thereby impacting the user comfort, injecting capacitive reactive power can be seen as an attractive

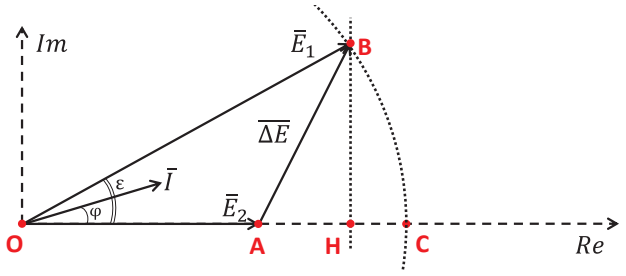

Fig. 3. Vector diagram.

alternative, thus operating in the IV quadrant of the EVSE converter charging capabilities in Fig. 2.

The main purpose of the proposed analysis is to provide guidelines for DSOs in terms of reactive power provision requirement for new EVSEs installation. Therefore, the determination of the effect of reactive power on the voltage at the end of the line as function of the installed apparent power is of high importance. For this reason, Eq. (9) has been combined with (4) and (5), in order to highlight separately the active power P and the reactive power Q, giving as result the formulation reported in Eq. (10) [32]. Note that (10) can be derived also directly from Eq. (7), without making explicit the real and imaginary current components I_r and I_i.

$$E_2 = \left\{\frac{1}{2}\left[E_1^2 - \frac{2}{3}(PR_l + QX_l) + \left(E_1^4 - \frac{4}{3}E_1^2(PR_l + QX_l) - \frac{4}{9}(PX_l + QR_l)^2\right)^{0.5}\right]\right\}^{0.5} \tag{10}$$

With (10) it is possible to calculate the voltage magnitude at the line ending terminal E_2, given the line parameters, the voltage at the source terminal, and the EV charging power in terms of P and Q.

Eq. (10) provides the expected phase-neutral voltage for fixed values of P and Q, thus considering that the actual absorbed power does not depend in any way on the local voltage. The assumption of considering no voltage-dependency, i.e., constant-power units, for new electrical installation is a common practice for grid operators when evaluating the grid impact of new eventual units (e.g., large loads, PVs, EVSEs). In fact, DSOs commonly consider the size of the new unit in terms of capacity, i.e., amount of power is going to be exchanged at the point of common coupling. For this reason, in this work the constant-power load model has been utilized for the new EV fast charger, whose size is indicated in terms of maximum charging power capacity.

By contrast, passive loads in power system are typically characterized by different voltage-dependency behaviours. According to the ZIP theory [36], each load can be modelled with reference to its nature: it can simply be a 'constant-power', a 'constant-voltage' or a 'constant-impedance' load, or it could be represented as a mix of the previous characteristics. A typical load representation is given by the polynomial model in Eqs. (11) and (12), which show voltage dependency of the actual absorbed active and reactive power P_{load} and Q_{load} according to the expected power values ($P_{load,0}$ and $Q_{load,0}$) in case of nominal local voltage $E_{2,0}$ of 230 V.

$$P_{load} = P_{load,0}\left[a_0 + a_1\frac{E_2}{E_{2,0}} + a_2\left(\frac{E_2}{E_{2,0}}\right)^2\right] \tag{11}$$

$$Q_{load} = Q_{Load,0}\left[b_0 + b_1\frac{E_2}{E_{2,0}} + b_2\left(\frac{E_2}{E_{2,0}}\right)^2\right] \tag{12}$$

Coefficients a_0, a_1, a_2 represent the shares of the constant-power, constant-current and constant-impedance contributions, respectively, and their sum is always equal to 1. The extreme cases of totally constant-power/current/impedance units are obtained by consider $a_i = 1$. Similar considerations are valid for coefficients b_0, b_1 and b_2, for the voltage-dependency of the reactive power. Typical ZIP coefficients for residential, industrial and commercial loads are reported in Section 5 [37].

The level of the investigation is now enhanced by considering the customer at the ending bus of Fig. 1 as a combination of certain load and the new EVSE. So, P and Q can be split in the two components relative to the EV (P_{EV} and Q_{EV}) and the load (P_{load} and Q_{load}), as shown in Eqs. (13) and (14).

$$P = P_{EV} + P_{load} \tag{13}$$

$$Q = Q_{EV} + Q_{load} \tag{14}$$

One can note that Eqs. (13) and (14) can be extended by including other types of units, such as inverter driven distributed energy resources. In this case, with reference to the ZIP modelling, the new P and Q power exchanged would be modelled as constant-power units.

If the voltage rises, on the one hand it is expected that a constant-power load would draw less current, thus enhancing the voltage regulation effect determined by reactive power provision. On the other hand, a constant-impedance load would consume more, thus reducing the effectiveness. Note that for the load the absorbed Q is typically inductive ($Q_{LOAD} > 0$), while for the charging EV it is generally capacitive ($Q_{EV} < 0$).

At this point, by combining Eq. (10) with (11)–(14), it is possible to derive the fourth order equation, shown in Eq. (15).

$$E_2^4 * \alpha + E_2^3 * \beta + E_2^2 * \gamma + E_2 * \delta + \xi = 0 \tag{15}$$

The coefficients $\{\alpha,\beta,\gamma,\delta,\xi\}$ are calculated as in Eqs. (16)–(20).

$$\alpha = 1 + \frac{2}{3E_{2,0}^2}(R_l P_{load,0} a_2 + X_l Q_{load,0} b_2) + \frac{1}{9E_{2,0}^4}(R_l^2 + X_l^2)[(P_{load,0} a_2)^2 + (Q_{load,0} b_2)^2] \tag{16}$$

$$\beta = \frac{2}{3E_{2,0}}(R_l P_{load,0} a_1 + X_l Q_{load,0} b_1) + \frac{1}{9E_{2,0}^3}(R_l^2 + X_l^2)(2P_{load,0}^2 a_1 a_2 + 2Q_{load,0}^2 b_1 b_2) \tag{17}$$

$$\gamma = -E_1^2 + \frac{2}{3}[R_l(P_{EV} + P_{load,0} a_0) - X_l(Q_{EV} + Q_{load,0} b_0)] + \frac{1}{9E_{2,0}^2}\{(R_l^2 + X_l^2)[(P_{load,0} a_1)^2 + 2P_{load,0}^2 a_0 a_2 + 2P_{EV} P_{load,0} a_2 + (Q_{load,0} b_1)^2 + 2Q_{load,0}^2 b_0 b_2 + 2Q_{EV} Q_{load,0} b_2]\} \tag{18}$$

$$\delta = \frac{1}{9E_{2,0}}(R_l^2 + X_l^2)(2P_{load,0}^2 a_0 a_1 + 2P_{EV} P_{load,0} a_1 + 2Q_{load,0}^2 b_0 b_1 + 2Q_{EV} Q_{load,0} b_1) \tag{19}$$

$$\xi = \frac{1}{9}(R_l^2 + X_l^2)[P_{EV}^2 + (P_{load,0} a_0)^2 + Q_{EV}^2 + (Q_{load,0} b_0)^2 + 2P_{EV} P_{load,0} a_0 + 2Q_{EV} Q_{load,0} b_0] \tag{20}$$

With (15), E_2 is calculated as function of the source voltage E_1, the line impedance, and the total active and reactive power, given a certain voltage-dependency of the load. With this formulation, the effect of the capacitive reactive power can be evaluated given a certain active power charging capacity P_{EV} of the new EVSE installation, by applying different Q_{EV}. In the proposed assessment analysis, the amount of reactive power Q_{EV} provided by the EVSE is determined by the power factor $\cos\varphi_{EV}$ set for the charging process, resulting in a fixed power factor operation mode, as commonly applied in small PV inverters. One can note that reactive power is provided only when the car is charging, i.e., when there is a need for a certain active power flow for the analysed voltage support control. So, for a given charging behaviour influenced by stochastic factors, the reactive power is to be seen as a mean to reduce the potential self-induced voltage issues, by constantly raising

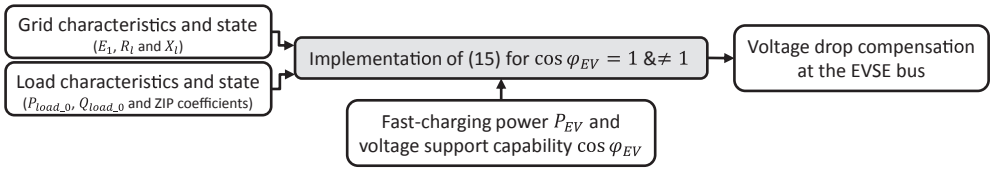

Fig. 4. Block diagram of the logic of the proposed method.

the bus voltage via a fixed cosφ logic. The control is completely decentralized and based merely on the implemented constant power factor logic, thus not including any centralized remote grid monitoring. The logic of the proposed methodology can be therefore summarized with the block diagram reported in Fig. 4.

The proposed formulation is a possible explicit formulation analytically derived by fundamental electrotechnical laws that gives the exact direct calculation of the voltage magnitude at the considered bus, with no need for iterative calculations as for the case of power flows calculation. The solution of Eq. (15) can be seen as a computationally simple and fast method able to provide a precise estimation of the voltage magnitude at the EVSE bus, with no need for iterative calculations.

3. Grid and components equivalent models

The first part of the investigation aims at evaluating the influence of the different power components (MV grid, MV/LV transformer, and LV cable) on the effectiveness of reactive power for voltage support, highlighting how much each component contributes to the total voltage drop. The single-line equivalent circuit in Fig. 5a is considered. The representation seen from the LV side is illustrated by the equivalent single-phase circuit with all the parameters referred to the 0.4 kV LV level $V_{n.LV}$. At this stage, no other loads are considered, thus only the impact of charging EVs with/without reactive power support is investigated. Fig. 5b shows the resistive and inductive components referred to the LV level of MV grid, MV/LV transformer, and LV feeder. These are termed and X_{grid}, R_{trafo} and X_{trafo}, and $R_{LVfeeder}$ and $X_{LVfeeder}$, respectively. With respect to the analysis in Section 2, the series of the three resistive and inductive components correspond to R_l and X_l of Fig. 1.

Typically, the $V_{n.MV}$ 10 kV MV grid's characteristics can be represented by the short-circuit power $S_{sc.grid}$ and the R/X_{grid} ratio: common values are 10 MVA and 0.5, respectively [33]. Through calculation of the short-circuit impedance $Z_{MVgrid.MV}$ and its components $R_{grid.MV}$ and $X_{grid.MV}$ the resistive and inductive components referred to the LV level and X_{grid} amount to 0.00716 Ω and 0.01431 Ω, respectively. The calculation is done using Eqs. (21)–(23).

$$Z_{grid.MV} = \frac{V_{n.MV}^2}{S_{sc.grid}} = (R_{grid.MV}^2 + X_{grid.MV}^2)^{0.5} \tag{21}$$

$$R_{grid} = R_{grid.MV}\left(\frac{V_{n.MV}}{V_{n.LV}}\right)^{-2} \tag{22}$$

$$X_{grid} = X_{grid.MV}\left(\frac{V_{n.MV}}{V_{n.LV}}\right)^{-2} \tag{23}$$

A typical MV/LV distribution power transformer is modelled in [30]. It is characterized by nominal apparent power $S_{n.trafo}$ of 0.4 MVA, short-circuit voltage $v_{sc\%.trafo}$ of 4%, and R/X_{trafo} ratio of 0.1. Via calculation of short-circuit power $S_{sc.trafo}$ and impedance $Z_{sc.trafo}$ – Eqs. (24) and (25) – the resistive and inductive components referred to the LV level R_{trafo} and X_{trafo} amount respectively to 0.00159 Ω and 0.0159 Ω.

$$S_{sc.trafo} = \frac{100 * S_{n.trafo}}{v_{sc\%.trafo}} \tag{24}$$

$$Z_{sc.trafo} = \frac{V_{n.LV}^2}{S_{sc.trafo}} = (R_{trafo}^2 + X_{trafo}^2)^{0.5} \tag{25}$$

This formulation does not include no-load current and no-load losses, which was found do not significantly impact the results. In particular, they only cause a minor off-set on the total voltage drop estimation of less than 0.1% of the nominal voltage.

Typical values of cable resistance and reactance per km are 0.163 and 0.136 Ω/km, respectively ($R/X_{LVfeeder}$ = 1.2, i.e., $X/R_{LVfeeder}$ = 0.8) [33]. The length of 1 km is chosen, as it can be considered as an upper limit of LV feeders length [38]. So, absolute $R_{LVfeeder}$ and $X_{LVfeeder}$ amount to 0.163 and 0.136 Ω, respectively.

Table 1 reports the considered typical values of power system components when modelling LV distribution grids. It also includes the related equivalent resistance and reactance referred to the LV level, with reference to the simplified single-phase equivalent circuit in Fig. 5b.

Eq. (10) has been implemented with E_1 set to 1 p.u. as for an ideal voltage source and P and Q equal to P_{EV} and Q_{EV}, respectively – only EVs as customer. Anyway, the aim of the study is assessing the voltage difference, thus the findings are still applicable also in other situations (i.e., higher voltages such as 1.05 because of reverse flow, or lower voltages such as 0.95 because of loaded feeders). One should also note that Eq. (10) could be implemented considering that the starting terminal of the line does not necessarily need to be at the MV grid or transformer level. Instead, it could be at any node of the distribution network. In this case, the ending terminal could be at the end of one of the branches derived from that very node.

Considering installation of new EVSEs with fast-charging capability up to 12.5 kW, it has been decided to assume a total EV active power demand of 50 kW, which represent a realistic case of 4 new EVSEs. Eq. (10) is implemented twice: with power factor cosφ_{EV} equal to 1 and then repeated with capacitive cosφ_{EV} equal to 0.9, and the difference ΔE_2 was evaluated as in Eq. (26).

Table 1
Standard parameters for distribution grids, adapted from [30] and [33].

	$S_{sc.grid}$ [MVA]	$S_{n.trafo}$ [MVA]	$v_{sc\%.trafo}$ [%]	R/X	R referred to LV level [Ω]	X referred to LV level [Ω]
MV grid [33]	10	–	–	0.5	0.00716	0.01431
MV/LV trafo [30]	–	0.4	4	0.1	0.00159	0.0159
LV feeder [33]	–	–	–	1.2	0.163	0.136

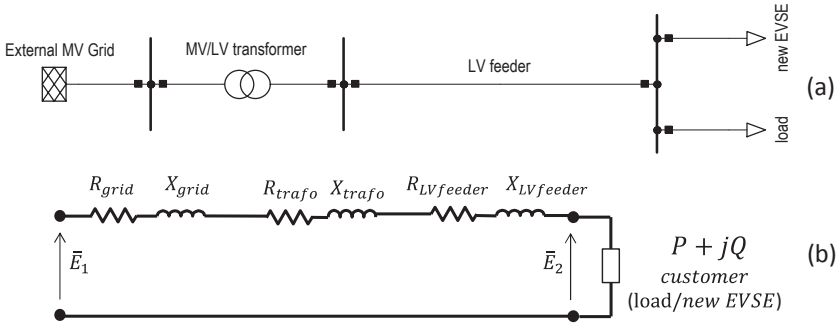

Fig. 5. Single-line (a) and single-phase equivalent circuit referred to the LV level (b) of a three-phase power system.

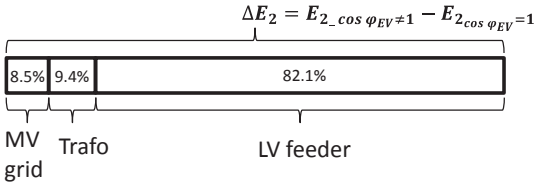

Fig. 6. Contribution to the reactive power effect on the voltage at the end of the line for each component.

$$\Delta E_2 = E_{2.\cos\varphi_{EV}\neq 1} - E_{2.\cos\varphi_{EV}=1} \quad (26)$$

The choice of considering a limit value of $\cos\varphi_{EV}$ of 0.9, is motivated by the fact that also in case of reactive power provision by PV inverters, the maximum reactive power exchange is limited by a power factor of 0.9 [10–12]. This value was identified as the maximum power factor that can be applied to the converter without excessive over-sizing. For this reason, the same value has been set for the EVSE inverters under analysis.

Considering the calculated constant values of the series resistive and inductive components of the circuit in Fig. 4b, a preliminary analysis of the influence of the three single components on the effects of reactive power is now presented. E_2 resulted in 0.9415 and 0.9673 p.u. for $\cos\varphi_{EV}$ equal to 1 and 0.9, respectively. It is clear that ΔE_2 (0.0258 p.u.) represents the voltage rise due to the reactive power injected by the EVs at the ending terminal of the line. The resulting ΔE_2 is obtained as effect of the three components. Specifically, the MV grid contributed 8.5%, the transformer 9.4%, while the LV feeder contributed 82.1%, as illustrated schematically in Fig. 6.

It is therefore found that the effect of the reactive power on the local voltage depends mainly on the characteristics of the LV feeder. This result was obtained considering one possible combination of typical distribution network components. Thus, it is of interest to see how different values of these components may impact the results. In this regards, the next part of the investigation aims at evaluating the single influence of the MV grid, the MV/LV transformer, and the LV feeder parameters.

4. Sensitivity analysis

4.1. Influence of the MV grid

The influence of the external MV grid is evaluated by calculating ΔE_2 first for different $S_{sc,grid}$ (1–10 MVA) and then for different R/X_{grid} (0.05–0.5), keeping constant the typical parameters of transformer and LV feeder of Table 1. Fig. 7a shows that the trend of ΔE_2 is influenced by the stiffness of the external MV grid, keeping, as in [33], the constant value of 0.5 for R/X_{grid}. In particular, for very weak grids results differ from the case of strong ones. Thus, hereafter all the studies consider two kinds of MV grid: weak and strong grid ($S_{sc,grid}$ = 2 and 10 MVA, respectively). Fig. 7b shows that in both the cases the effect of reactive power on the ending terminal voltage is constant for all the considered R/X_{grid} ratios. Thus, hereafter the constant value of 0.5 for R/X_{grid} is used.

4.2. Influence of the distribution MV/LV transformer

The influence of the distribution MV/LV transformer is evaluated by calculating ΔE_2 for different $S_{n,trafo}$ (0.1–1 MVA), keeping constant the typical values of $v_{sc\%,trafo}$, R/X_{trafo} and LV feeder, as in Table 1. The analysis is carried out for weak and strong MV grid. Fig. 8 shows that the influence of the transformer on the effect of reactive power is marginal for $S_{n,trafo} \geq 0.2$ MVA, while for smaller sizes, the contribution becomes noticeable. As the grid model considers a LV feeder at the secondary side of the transformer, it is to be expected that in addition to the new EVSEs at the line end, distributed loads are connected along the feeder. Thus, as in this study a realistic case of new EVSEs installation for a total of 50 kW is considered, a minimum size of 0.2 MVA has to be considered for the transformer. For this reason, hereafter the typical values of the MV/LV transformer reported in Table 1 are considered and kept constant, as its influence on the effect of the reactive power is considered marginal.

4.3. Influence of the LV feeder

The influence of the LV feeder is evaluated by calculating ΔE_2 first

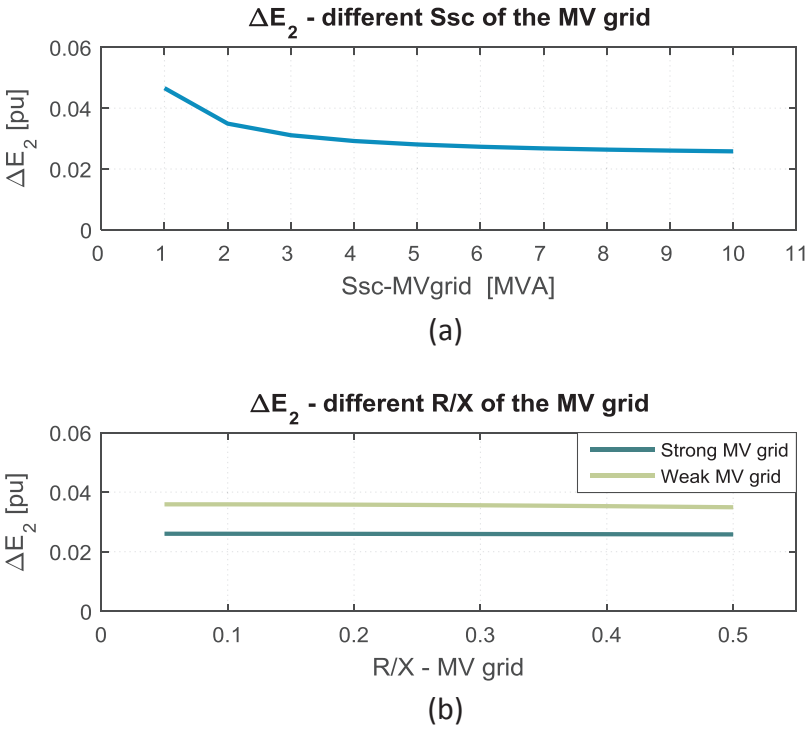

Fig. 7. Influence of MV grid for $\cos\varphi_{EV\neq 1} = 0.9$.

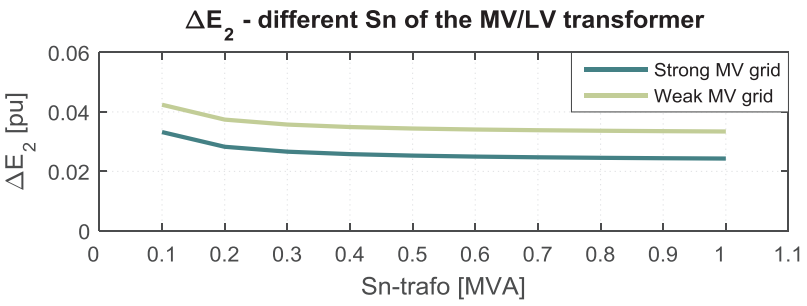

Fig. 8. Influence of the MV/LV transformer for $\cos\varphi_{EV\neq 1} = 0.9$.

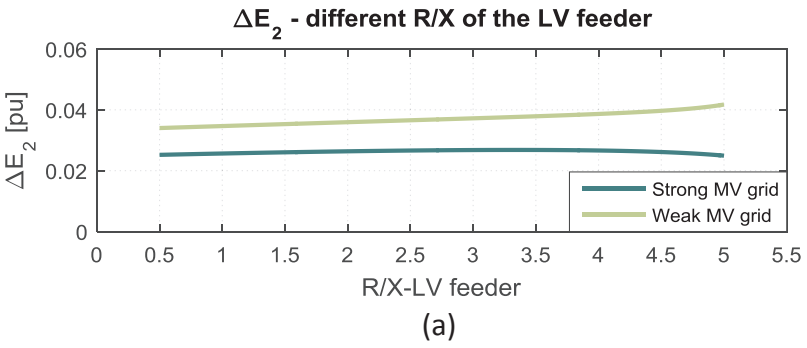

Fig. 9. Influence of the LV feeder for $\cos\varphi_{EV\neq 1} = 0.9$.

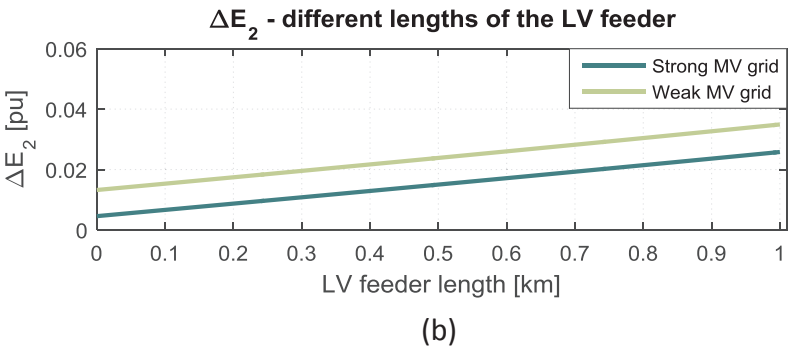

for different $R/X_{LVfeeder}$ and then for different lengths, considering both weak and strong MV grid, and the MV/LV transformer from Table 1. Since it is known that the reactance per km is usually constant for different kinds of cables, for the first case different $R/X_{LVfeeder}$ are obtained by varying the value of the resistive component (0.07–0.7 Ω/km), i.e., by considering different sections of the cable conductors, keeping the length equal to 1 km [38]. For the case of different lengths (0–1 km), the values per km reported in Table 1 are used and kept constant. Fig. 9a shows that for different $R/X_{LVfeeder}$, ΔE_2 results relatively constant, while from Fig. 9b it is possible to deduce that the main influence is given by the absolute values of $R_{LVfeeder}$ and $X_{LVfeeder}$, i.e., by the length.

It is found that the main influence of reactive power on the voltage support is determined by the absolute values of the LV feeder impedance, i.e., by the length, rather than by the $R/X_{LVfeeder}$ ratio.

4.4. Voltage rise as function of cos(φ_{EV}) and length

It is clear that ΔE_2 depends on the amount of the capacitive reactive power provided by the EV, i.e., on the power factor $\cos\varphi_{EV}$ set by the EVSE. Therefore, the last formulation proposed in this Section considers ΔE_2 as function of the LV feeder length and $\cos\varphi_{EV}$, varied between 0.9 and 1.

Table 2 presents numerical results for the case of the strong MV grid, i.e., the most common one. As expected, the effectiveness of the reactive power on voltage support is increasing with decreasing power factor, up to the maximum value of 0.0258 p.u. for standard LV feeder length of 1 km, for strong MV grid. Moreover, it is noticeable that for any given $\cos\varphi_{EV}$, the effects are linearly dependent on the absolute value of the LV feeder impedance (thus the length), as previously demonstrated.

4.5. Inclusion of voltage-dependent loads

The analysis presented so far has not considered any loading except for the new EVSE itself, in fact Eq. (10) was implemented considering only EVs as customer. Now the investigation is enhanced through the implementation of (15), for different voltage-dependent loads in

Table 2
ΔE_2 for different $\cos\varphi_{EV}$ – length combinations.

		$\cos\varphi_{EV}$					
		1	0.98	0.96	0.94	0.92	0.9
Length [km]	0.2	0	0.0037	0.0053	0.0066	0.0077	0.0087
	0.4	0	0.0055	0.0078	0.0097	0.0114	0.0129
	0.6	0	0.0073	0.0104	0.0129	0.0151	0.0171
	0.8	0	0.0092	0.0131	0.0162	0.0189	0.0214
	1.0	0	0.0111	0.0158	0.0195	0.0228	0.0258

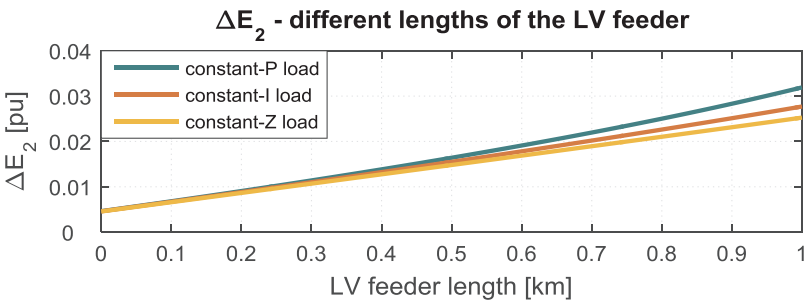

Fig. 10. Voltage rise effect of the reactive power provided by EVs for $\cos\varphi_{EV\neq1} = 0.9$, as function of the LV feeder length for different voltage-dependency of loads, for strong MV grid.

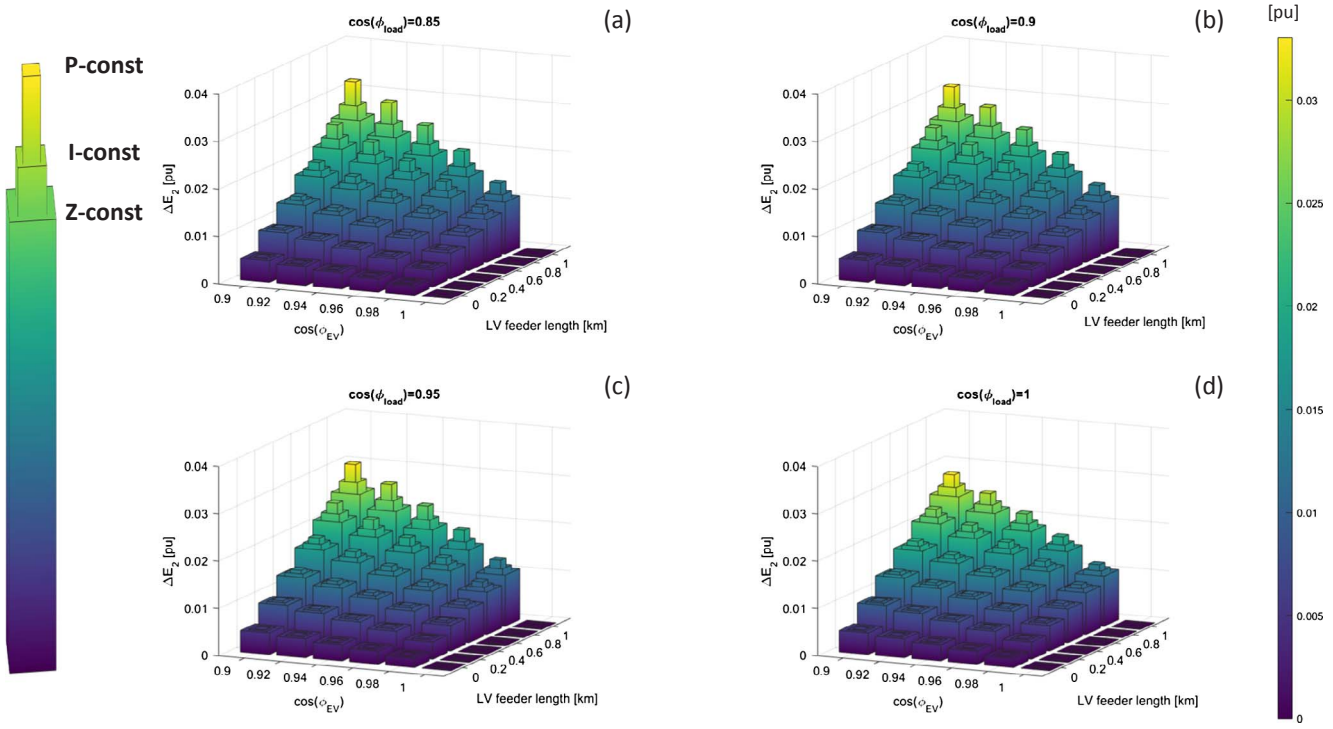

Fig. 11. Voltage rise effect of the reactive power provided by EVs as function of the LV feeder length and $\cos\varphi_{EV}$, for different voltage-dependent loads and for $\cos\varphi_{load} = 0.85$, 09, 0.95, 1 in (a), (b), (c) and (d), respectively.

addition to the EVs. The nominal active power $P_{load,0}$ is kept constantly equal to 50 kW, while different load types and different amount of inductive reactive power active power $Q_{load,0}$ (i.e., different values of $\cos\varphi_{load}$) are considered.

Fig. 10 shows the effect of capacitive reactive power provided from EVs on the voltage at the ending terminal of the feeder for different load types (constant P, I or Z). In this case, the comparison is done for $\cos\varphi_{EV\neq1} = 0.9$, considering constant $\cos\varphi_{load} = 0.9$. It can be noticed that the load type influences the results for lines longer than 0.4 km, with more evident effects in case of no voltage-dependency (constant-P load) rather than for voltage-dependent load. Specifically, for a 1 km line, ΔE_2 amounts to 0.0319, 0.0277 and 0.0253 for constant-P, constant-I and constant-Z loads, respectively. Although an exhaustive sensitivity analysis would require load models with mixed coefficients, the results of the three analyzed load types represent the extreme cases. In fact, by using mixes of the coefficients, intermediate results would be obtained.

Similarly to the analysis reported in Section 4.4, it is of interest to evaluate ΔE_2 as function of the LV feeder length and $\cos\varphi_{EV}$, varied between 0.9 and 1, for the three different load types.

Fig. 11 shows 3D bar plots of ΔE_2 for the three different load types and $\cos\varphi_{load}$ equal 0.85, 0.9, 0.95 and 1, in subfigures (a), (b), (c) and (d), respectively. Note that the three different widths of the bars indicate the load type, in particular, the widest one is for constant-Z loads, the middle one for constant-I loads, while the tightest one for constant-P loads.

As expected, Fig. 11 shows that the more the load is voltage dependent, the smaller is the contribution of the capacitive reactive power in rising the voltage. In fact, as shown in Fig. 10 in case of constant-P load, ΔE_2 is higher than in the case of constant-I load, which is higher than in the case of constant-Z load. Furthermore, as demonstrated in Section 4.4, ΔE_2 is higher with decreasing amount of the capacitive reactive power provided by the EV, i.e., with decreasing $\cos\varphi_{EV}$.

Table 3 presents numerical results of the cases of highest reactive power contribution from EVs, i.e., the case of $\cos\varphi_{EV\neq1} = 0.9$. Results confirm the linear trend with the LV feeder length, and show less voltage support effects in case of higher load power factors $\cos\varphi_{load}$.

5. Validation on typical LV distribution grids

This Section reports a validation of the proposed method on the reference Cigrè European LV distribution feeder [33] as well as on a real Danish LV distribution network previously utilized for other EV integration-related studies [30]. Simulations are carried out both applying the proposed formulation and by means of DIgSILENT PowerFactory load flows. For the implementation of Eqs. (11) and (12), the

Table 3
ΔE_2 for different lengths – load model combinations with $\cos\varphi_{EV\neq1} = 0.9$.

		Constant-P load	Constant-I load	Constant-Z load
		$\cos\varphi_{load} = 0.85$		
Length [km]	0.2	0.0091	0.0089	0.0087
	0.4	0.0140	0.0133	0.0128
	0.6	0.0194	0.0180	0.0169
	0.8	0.0256	0.0229	0.0212
	1.0	0.0330	0.0282	0.0254
		$\cos\varphi_{load} = 0.9$		
Length [km]	0.2	0.0091	0.0088	0.0086
	0.4	0.0138	0.0132	0.0127
	0.6	0.0191	0.0178	0.0169
	0.8	0.0250	0.0226	0.0210
	1.0	0.0319	0.0277	0.0253
		$\cos\varphi_{load} = 0.95$		
Length [km]	0.2	0.0090	0.0088	0.0086
	0.4	0.0137	0.0131	0.0127
	0.6	0.0187	0.0176	0.0168
	0.8	0.0243	0.0223	0.0209
	1.0	0.0308	0.0272	0.0250
		$\cos\varphi_{load} = 1$		
Length [km]	0.2	0.0089	0.0087	0.0086
	0.4	0.0133	0.0129	0.0126
	0.6	0.0180	0.0172	0.0166
	0.8	0.0231	0.0216	0.0206
	1.0	0.0286	0.0262	0.0246

Table 4
Standard parameters for distribution grids, adapted from [37].

	a_0	a_1	a_2	b_0	b_1	b_2
Residential	1.27	−1.12	0.85	8.77	−18.73	10.96
Industrial	1	0	0	1	0	0
Large commercial	1.06	−0.53	0.47	4.43	−8.73	5.30
Small commercial	0.63	−0.06	0.43	3.59	−6.65	4.06

typical ZIP coefficients for residential load class have been utilized, which are reported in Table 4 along with industrial and commercial load classes.

5.1. Cigrè European LV reference grid

The residential reference Cigrè European LV distribution feeder is schematized in Fig. 12. Installation of four new 12.5 kW EVSEs (for a total of 50 kW) is considered at buses 2–6, which are, case by case, the ending terminal bus with respect to the formulation proposed in Section 3. The loading and the single-feeder characteristics (transformer-bus) are in Table 5.

Due to the limited length of the line, results are not expected to be dramatically influenced by the voltage dependency of the loads type. However, the typical ZIP coefficients for residential load class indicated in Table 4 are utilized. Results are reported in Table 6, which shows voltage E_2 for unitary $\cos\varphi_{EV}$, for $\cos\varphi_{EV} = 0.9$, and the difference ΔE_2 in case of 50 kW of EVs charging at buses 2–6.

Table 5
Properties of the Cigrè transformer-bus feeder and loading at each bus.

Bus	Total length [m]	$R/X_{LVfeeder}$	$P_{load,0}$ [kW]	$\cos\varphi_{load}$
B2	95	3.67	5.13	0.9
B3	240	2.08	51.3	0.9
B4	205	1.57	22.5	0.9
B5	310	2.08	5.13	0.9
B6	345	1.74	22.5	0.9

Table 6
Results from validation analyses on the Cigrè grid for 50 kW EVSE connected at the different buses.

Bus	Proposed method			Power flow in powerfactory		
	E_2 [p.u.]		ΔE_2	E_2 [p.u.]		ΔE_2
	$\cos\varphi_{EV} = 1$	$\cos\varphi_{EV} = 0.9$		$\cos\varphi_{EV} = 1$	$\cos\varphi_{EV} = 0.9$	
B2	0.9760	0.9825	0.0065	0.9760	0.9825	0.0065
B3	0.9491	0.9587	0.0096	0.9491	0.9587	0.0096
B4	0.9711	0.9796	0.0085	0.9711	0.9796	0.0085
B5	0.9629	0.9738	0.0109	0.9629	0.9738	0.0109
B6	0.9508	0.9626	0.0118	0.9508	0.9626	0.0118

As deducible from Table 6, the results from the implementation of the proposed method respect very accurately the ones obtained carrying out iterative power flow simulations in DIgSILENT PowerFactory. This is true given a sufficiently small tolerance (equal to 0.1 kVA) when solving Newton-Rapson calculations. In this case the difference between the results from the two methods is smaller than 0.01%. In case of larger tolerance the convergence might still be obtained, though with minor differences in the results, as less iterations would be needed due to the less tight tolerance. Moreover, the expected trend of growing ΔE_2 with the line length independently from the $R/X_{LVfeeder}$ ratio demonstrated in Section 4 is confirmed.

5.2. Real Danish LV distribution grid

As for the validation on the real Danish LV grid, the schematic is shown in Fig. 13, and the installation of four new 12.5 kW EVSEs (for a total of 50 kW) is considered cyclically at each bus from 602 to 613. The voltage values of the EVSE bus is E_2 in the proposed formulation (Eq. (15)), which corresponds to the ending terminal bus with reference to the diagram on Fig. 5. The loading and the single-feeder characteristics (transformer-bus) are in Table 7. It has been decided to simulate the

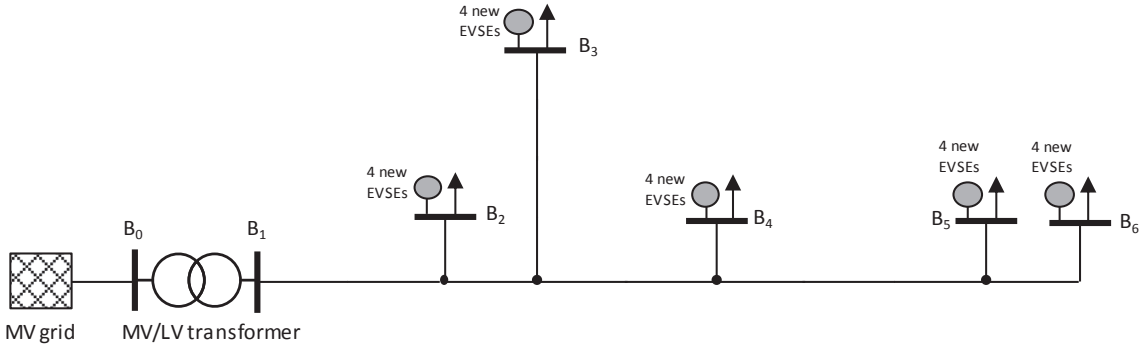

Fig. 12. Single-phase circuit of the modelled Cigrè distribution grid under study.

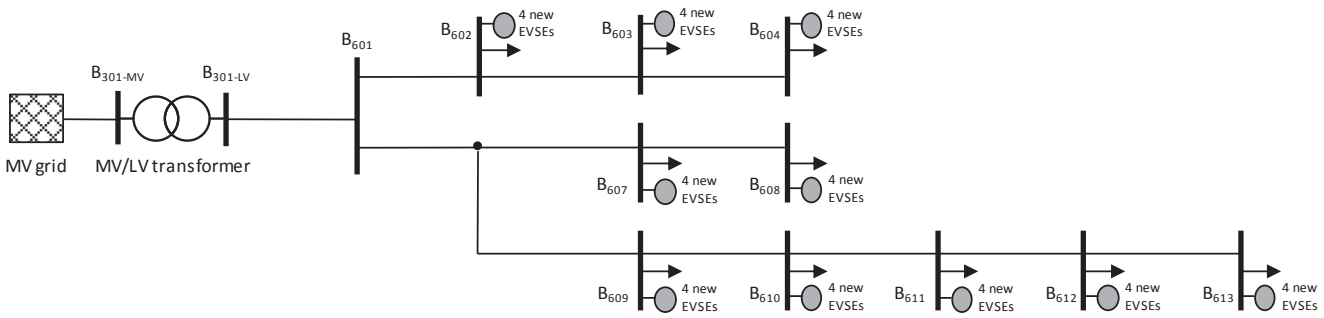

Fig. 13. Single-phase circuit of the modelled Danish distribution grid under study.

Table 7
Properties of the real Danish LV grid transformer-bus feeder and loading at each bus.

Bus	Total length [m]	$R/X_{LVfeeder}$	P_{load0} [kW]	$\cos\varphi_{load}$
B601	112	2.8	0	–
B602	161	2.8	8.21	0.95
B603	225	2.8	5.48	0.95
B604	312	2.8	11.88	0.95
B607	263	2.8	16.14	0.95
B608	300	2.8	11.19	0.95
B609	257	2.8	9.98	0.95
B610	292	2.8	13.71	0.95
B611	328	2.8	13.85	0.95
B612	363	2.8	14.18	0.95
B613	398	2.8	12.59	0.95

worst case of maximum loading condition of a winter week, when high load demand is present due to heat pumps heating systems, while there is no PV production due to weather conditions.

Again, the typical ZIP coefficients for residential load class in Table 4 are utilized. Results are reported in Table 8, which shows voltage E_2 for unitary $\cos\varphi_{EV}$, for $\cos\varphi_{EV} = 0.9$, and the difference ΔE_2 in case of 50 kW of EVs charging at all the buses.

The results obtained from the implementation of the proposed formulation respect very accurately the ones obtained carrying out power flow simulations in DIgSILENT PowerFactory. Again, the sufficiently small tolerance (equal to 0.1 kVA) utilized when solving power flow calculations enables the results to look identical, as difference smaller than 0.01% are obtained. As in this case the cable lines of the modelled network are all of the same type, they have the same $R/X_{LVfeeder}$ ratio. Nonetheless, the expected trend of growing ΔE_2 with the line length is confirmed.

6. Conclusions and future works

The aim of the work was to analyse the potentials of reactive power provision by EVSEs on voltage support, depending on grid's and load's characteristics. This is considered as a possible mean of evaluation for the DSO when assessing the grid impact of new fast charging EVSEs and the respective flexibility in terms of voltage control. An analytical formulation is proposed to calculate the expected voltage at the ending-terminal of a distribution line given as input the grid characteristic, the load and its voltage-dependency.

The considered simplified distribution grid is composed by an external MV grid, a MV/LV distribution transformer, and a single radial LV line, and all their impedances have been referred to the LV level. Considering multiple values of the parameters of all the components, it was found that the effect of the capacitive reactive power is influenced mostly by the stiffness of the external MV grid and by the absolute values of the LV feeder impedance. Specifically, it was found that the R/X ratio of the LV feeder did not significantly influence the results, while its absolute impedance was crucial. Since the LV cable reactance per km

Table 8
Results from validation on the real Danish grid for 50 kW EVSE connected at the different buses.

Bus	Proposed method			Power flow in powerfactory		
	E_2 [p.u.]		ΔE_2	E_2 [p.u.]		ΔE_2
	$\cos\varphi_{EV} = 1$	$\cos\varphi_{EV} = 0.9$		$\cos\varphi_{EV} = 1$	$\cos\varphi_{EV} = 0.9$	
B602	0.9866	0.9908	0.0042	0.9866	0.9908	0.0042
B603	0.9826	0.9875	0.0049	0.9826	0.9875	0.0049
B604	0.9728	0.9787	0.0059	0.9728	0.9787	0.0059
B607	0.9751	0.9805	0.0054	0.9751	0.9805	0.0054
B608	0.9741	0.9799	0.0058	0.9742	0.9800	0.0058
B609	0.9783	0.9836	0.0053	0.9783	0.9836	0.0053
B610	0.9736	0.9793	0.0057	0.9736	0.9793	0.0057
B611	0.9704	0.9765	0.0061	0.9704	0.9765	0.0062
B612	0.9670	0.9736	0.0066	0.9670	0.9735	0.0065
B613	0.9649	0.9718	0.0069	0.9649	0.9718	0.0069

is substantially constant for most cross sections, the variety of the absolute values was obtained by considering different cable lengths.

It was found that results are influenced by the load voltage-dependency only for lines longer than 400 m. In particular, the more the load is voltage dependent, the smaller is the contribution of the capacitive reactive power in rising the voltage, and vice versa. In fact, in case of constant-power loads the studied EV voltage support is more effective than in case of constant-impedance-load.

With the proposed formulation the DSO is able to assess the voltage drop compensation due to the application of a particular power factor by the EV fast charger as function of the LV feeder length, given as input the EVSE installed power and the load condition. In this way, DSOs can clearly evaluate the effect of the reactive power for any of their LV feeders when the power absorbed by EVs chargers would cause unacceptable under-voltages.

Results showed that for an autonomous decentralized reactive power provision control embedded in the new fast charging EVSE, the voltage support to the DSO is limited by the technical characteristics of the feeder. In particular, the proposed validation analysis on realistic LV feeders for the case of a fixed capacitive power factor of 0.9 proves that the voltage rise would amount to 0.012 p.u., in comparison to the case of EV charging with unitary power factor. The authors recognize that such voltage drop reductions can potentially avoid the violation of voltage thresholds, thus assuring compliance with grid technical standards on voltage levels. At any rate, this precaution may not be sufficient for massive penetration of EVSEs, since a combination with other smart charging strategies such as charging modulation and/or charging shifting may be essential for prevention of unacceptable under-voltage conditions. In conclusion, the authors believe that reactive power solutions is to be seen as a possible connection capability requirement, able to mitigate the self-induced negative effects of fast charging EVs in LV distribution grids, similarly to the current requirements for new PV

system installation in many European countries. In this regard, reactive power capabilities are required by the newly released Danish technical standard for stationary storage systems including vehicle-to-grid EV charging station [39].

Future research works should cover the investigation of reactive power provision in unbalanced distribution grids. In this case, the approach to the problem would be slightly different, as the DSO analysis would not be aiming at evaluating permission for installation of new EVSE with fast-charging capability, instead the focus would be on the effects of unbalanced voltage support by capacitive reactive power provision by single-phase EVs.

Acknowledgments

The authors would like to acknowledge the support of the EUDP (Denmark) funded project ACES – Across Continents Electric Vehicle Services (Grant EUDP17-I-12499, website: www.aces-bornholm.eu).

Appendix A. Supplementary material

Supplementary data associated with this article can be found, in the online version, at http://dx.doi.org/10.1016/j.ijepes.2017.10.034.

References

[1] Izadkhast S, Garcia-Gonzalez P, Frías P. An aggregate model of plug-in electric vehicles for primary frequency control. IEEE Trans Power Syst 2015;30:1475–82. http://dx.doi.org/10.1109/TPWRS.2014.2337373.
[2] Zecchino A, Rezkalla M, Marinelli M. Grid frequency support by single-phase electric vehicles : fast primary control enhanced by a stabilizer algorithm. In: 2016 Universities power engineering conference (UPEC), Coimbra, Portugal; 2016. p. 1–6.
[3] González Vayá M, Andersson G. Combined smart-charging and frequency regulation for fleets of plug-in electric vehicles. in: 2013 IEEE power & energy society general meeting, Vancouver, BC; 2013. p. 1–5. http://dx.doi.org/10.1109/PESMG.2013.6672852.
[4] Knezović K, Martinenas S, Andersen PB, Zecchino A, Marinelli M. Enhancing the role of electric vehicles in the power grid: field validation of multiple ancillary services. IEEE Trans Transport Electrificat 2016;3:201–9. http://dx.doi.org/10.1109/TTE.2016.2616864.
[5] Martinenas S, Knezović K, Marinelli M. Management of power quality issues in low voltage networks using electric vehicles: experimental validation. IEEE Trans Power Delivery 2016;8977:1–9. http://dx.doi.org/10.1109/TPWRD.2016.2614582.
[6] Clement-Nyns K, Haesen E, Driesen J. The impact of vehicle-to-grid on the distribution grid. Electr Power Syst Res 2011;81:185–92. http://dx.doi.org/10.1016/j.epsr.2010.08.007.
[7] Rodriguez-Calvo A, Cossent R, Frías P. Integration of PV and EVs in unbalanced residential LV networks and implications for the smart grid and advanced metering infrastructure deployment. Int J Electr Power Energy Syst 2017;91:121–34. http://dx.doi.org/10.1016/j.ijepes.2017.03.008.
[8] European Technical Standard EN 50160; 2011.
[9] Kechroud A, Ribeiro PF, Kling WL. Distributed generation support for voltage regulation: An adaptive approach. Electr Power Syst Res 2014;107:213–20. http://dx.doi.org/10.1016/j.epsr.2013.09.004.
[10] Italian Technical Standard CEI 0-21 Rules for the connection to the LV electrical utilities; 2012.
[11] German Technical Standard VDE-AR-N 4105 Power generation systems connected to the low-voltage distribution network; 2011.
[12] Energinet.dk, Danish Technical Regulation 3.2.2 for PV power plants with a power output above 11 kW; 2015.
[13] Caldon R, Coppo M, Turri R. Distributed voltage control strategy for LV networks with inverter-interfaced generators. Electr Power Syst Res 2014;107:85–92. http://dx.doi.org/10.1016/j.epsr.2013.09.009.
[14] Hu J, Marinelli M, Coppo M, Zecchino A, Bindner HW. Coordinated voltage control of a decoupled three-phase on-load tap changer transformer and photovoltaic inverters for managing unbalanced networks. Electr Power Syst Res 2016;131:264–74. http://dx.doi.org/10.1016/j.epsr.2015.10.025.
[15] Kisacikoglu MC, Kesler M, Tolbert LM. Single-phase on-board bidirectional PEV charger for V2G reactive power operation. IEEE Trans Smart Grid 2015;6:767–75.
[16] Ferreira RJ, Miranda LM, Ara RE. A new bi-directional charger for vehicle-to-grid integration. In: Innovative smart grid technologies (ISGT Europe), 2011 2nd IEEE PES international conference and exhibition O, Manchester, UK; 2011.
[17] Kisacikoglu MC, Ozpineci B, Tolbert LM. Reactive power operation analysis of a single-phase EV/PHEV bidirectional battery charger. In: 8th International conference on power electronics (ECCE), Jeju, Korea; 2011. p. 585–92.
[18] Kisacikoglu MC, Ozpineci B, Tolbert LM. Examination of a PHEV bidirectional charger system for V2G reactive power compensation. In: Proc IEEE APEC exposition, palm springs, CA, USA; 2010. p. 458–65.
[19] Kesler M, Kisacikoglu MC, Tolbert LM. Vehicle-to-grid reactive power operation using plug-in electric vehicle bidirectional off board charger. IEEE Trans Industr Electron 2014;61:6778–84.
[20] De Souza BA, Márcio A, De Almeida F. Multiobjective optimization and fuzzy logic applied to planning of the volt/var problem in distributions systems. IEEE Trans Power Syst 2010;25:1274–81.
[21] Huang W, Gan D, Xia X, Kobayashi N, Xu X. Distributed generation on distribution system voltage regulation : an optimization-based approach. In: Power and energy society general meeting, 2010 IEEE, Providence, RI, USA; 2010. p. 1–7.
[22] Manbachi M, Farhangi H, Palizban A, Arzanpour S. A novel volt-VAR optimization engine for smart distribution networks utilizing vehicle to grid dispatch. Int J Electr Power Energy Syst 2016;74:238–51. http://dx.doi.org/10.1016/j.ijepes.2015.07.030.
[23] Fakham H, Ahmidi A, Colas F, Guillaud X. Multi-agent system for distributed voltage regulation of wind generators connected to distribution network. In: Proc innovative smart grid technologies conference Europe (ISGT Europe), IEEE PES, Gothenburg, Sweden; 2010. p. 1–6.
[24] Morvaj B, Knezović K, Evins R, Marinelli M. Integrating multi-domain distributed energy systems with electric vehicle PQ flexibility: optimal design and operation scheduling for sustainable low-voltage distribution grids. Sustain Energy, Grids Networks 2016;8:51–61. http://dx.doi.org/10.1016/j.segan.2016.10.001.
[25] García-Villalobos J, Zamora I, Knezović K, Marinelli M. Multi-objective optimization control of plug-in electric vehicles in low voltage distribution networks. Appl Energy 2016;180:155–68. http://dx.doi.org/10.1016/j.apenergy.2016.07.110.
[26] Leemput N, Geth F, Van Roy J, Büscher J, Driesen J. Reactive power support in residential LV distribution grids through electric vehicle charging. Sustain Energy, Grids Networks 2015;3:24–35. http://dx.doi.org/10.1016/j.segan.2015.05.002.
[27] Kohrs R, Dallmer-Zerbe K, Mierau M, Wittwer C. Autonomous reactive power control by electric vehicles. In: Innovative smart grid technologies conference Europe (ISGT-Europe), 2014 IEEE PES, Istanbul, Turkey; 2014. p. 1–6. http://dx.doi.org/10.1109/ISGTEurope.%202014.7028771.
[28] Ying J, Ramachandaramurthy VK, Miao K, Mithulananthan N. Bi-directional electric vehicle fast charging station with novel reactive power compensation for voltage regulation. Int J Electr Power Energy Syst 2015;64:300–10. http://dx.doi.org/10.1016/j.ijepes.2014.07.025.
[29] Krasselt P, Suriyah MR, Leibfried T. Reactive power support for optimal grid integration of fast-charging infrastructure in german low-voltage networks. In: 23rd International conference on electricity distribution (CIRED), Lyon, France; 2015. p. 1–5.
[30] Knezović K, Marinelli M. Phase-wise enhanced voltage support from electric vehicles in a Danish low-voltage distribution grid. Electr Power Syst Res 2016;140:274–83. http://dx.doi.org/10.1016/j.epsr.2016.06.015.
[31] Winter C, Schwalbe R, Heidl M, Prüggler W. Harnessing PV inverter controls for increased hosting capacities of smart low voltage grids recent results from Austrian research and demonstration projects. In: 4th International workshop on integration of solar power into power systems, Berlin, Germany; 2014. p. 1–6.
[32] Zecchino A, Marinelli M, Korpås M, Træholt C. Guidelines for distribution system operators on reactive power provision by electric vehicles in low voltage grids. CIRED, Open Access Proc. J. 2017. p. 1–5. http://dx.doi.org/10.1049/oap-cired.2017.0377.
[33] Strunz K. CIGRE task force C6.04.02 – benchmark systems for network integration of renewable and distributed energy resources; 2009.
[34] NISSAN, Nissan, enel and nuvve operate world's first fully commercial vehicle-to-grid hub in Denmark, http://www.nissan-Helsingor.dk/index.php/om-os/nyheder/show/news/id/4; 2016.
[35] Haque MH. Load flow solution of distribution systems with voltage dependent load models. Electr Power Syst Res 1996;36:151–6. http://dx.doi.org/10.1016/0378-7796(95)01025-4.
[36] Price WW. IEEE task force on load representation for dynamic performance, load representation for dynamic performance analysis. IEEE Trans Power Syst 1993;8:472–82.
[37] Diaz-Aguiló M, Sandraz J, Macwan R, de León F, Member S, Czarkowski D, et al. Field-validated load model for the analysis of CVR in distribution secondary networks: energy conservation. IEEE Trans Power Delivery 2013;28:2428–36. http://dx.doi.org/10.1109/TPWRD.2013.2271095.
[38] Lehfuss F, Kadam S, Rodriguez Sanchez R. COTEVOS – specification of reference electricity networks; 2014.
[39] Energinet.dk, Danish Technical regulation 3.3.1 for battery plants; 2017.